DESY 06-023 ISSN 0418-9833
March 2006

# Diffractive Photoproduction of $\rho$ Mesons with Large Momentum Transfer at HERA

H1 Collaboration

**Abstract**

The diffractive photoproduction of $\rho$ mesons, $ep \rightarrow e\rho Y$, with large momentum transfer squared at the proton vertex, $|t|$, is studied with the H1 detector at HERA using an integrated luminosity of $20.1~\mathrm{pb}^{-1}$. The photon-proton centre of mass energy spans the range $75 < W < 95$ GeV, the photon virtuality is restricted to $Q^2 < 0.01~\mathrm{GeV}^2$ and the mass $M_Y$ of the proton remnant is below 5 GeV. The $t$ dependence of the cross section is measured for the range $1.5 < |t| < 10.0~\mathrm{GeV}^2$ and is well described by a power law, $\mathrm{d}\sigma/\mathrm{d}|t| \propto |t|^{-n}$. The spin density matrix elements, which provide information on the helicity structure of the interaction, are extracted using measurements of angular distributions of the $\rho$ decay products. The data indicate a violation of $s$-channel helicity conservation, with contributions from both single and double helicity-flip being observed. The results are compared to the predictions of perturbative QCD models.

Submitted to *Phys. Lett.* **B**

A. Aktas[9], V. Andreev[25], T. Anthonis[3], B. Antunovic[26], S. Aplin[9], A. Asmone[33], A. Astvatsatourov[3], A. Babaev[24,†], S. Backovic[30], A. Baghdasaryan[37], P. Baranov[25], E. Barrelet[29], W. Bartel[9], S. Baudrand[27], S. Baumgartner[39], J. Becker[40], M. Beckingham[9], O. Behnke[12], O. Behrendt[6], A. Belousov[25], N. Berger[39], J.C. Bizot[27], M.-O. Boenig[6], V. Boudry[28], J. Bracinik[26], G. Brandt[12], V. Brisson[27], D. Bruncko[15], F.W. Büsser[10], A. Bunyatyan[11,37], G. Buschhorn[26], L. Bystritskaya[24], A.J. Campbell[9], F. Cassol-Brunner[21], K. Cerny[32], V. Cerny[15,46], V. Chekelian[26], J.G. Contreras[22], J.A. Coughlan[4], B.E. Cox[20], G. Cozzika[8], J. Cvach[31], J.B. Dainton[17], W.D. Dau[14], K. Daum[36,42], Y. de Boer[24], B. Delcourt[27], M. Del Degan[39], A. De Roeck[9,44], E.A. De Wolf[3], C. Diaconu[21], V. Dodonov[11], A. Dubak[30,45], G. Eckerlin[9], V. Efremenko[24], S. Egli[35], R. Eichler[35], F. Eisele[12], A. Eliseev[25], E. Elsen[9], S. Essenov[24], A. Falkewicz[5], P.J.W. Faulkner[2], L. Favart[3], A. Fedotov[24], R. Felst[9], J. Feltesse[8], J. Ferencei[15], L. Finke[10], M. Fleischer[9], P. Fleischmann[9], G. Flucke[33], A. Fomenko[25], G. Franke[9], T. Frisson[28], E. Gabathuler[17], E. Garutti[9], J. Gayler[9], C. Gerlich[12], S. Ghazaryan[37], S. Ginzburgskaya[24], A. Glazov[9], I. Glushkov[38], L. Goerlich[5], M. Goettlich[9], N. Gogitidze[25], S. Gorbounov[38], C. Grab[39], T. Greenshaw[17], M. Gregori[18], B.R. Grell[9], G. Grindhammer[26], C. Gwilliam[20], D. Haidt[9], L. Hajduk[5], M. Hansson[19], G. Heinzelmann[10], R.C.W. Henderson[16], H. Henschel[38], G. Herrera[23], M. Hildebrandt[35], K.H. Hiller[38], D. Hoffmann[21], R. Horisberger[35], A. Hovhannisyan[37], T. Hreus[3,43], S. Hussain[18], M. Ibbotson[20], M. Ismail[20], M. Jacquet[27], L. Janauschek[26], X. Janssen[3], V. Jemanov[10], L. Jönsson[19], D.P. Johnson[3], A.W. Jung[13], H. Jung[19,9], M. Kapichine[7], J. Katzy[9], I.R. Kenyon[2], C. Kiesling[26], M. Klein[38], C. Kleinwort[9], T. Klimkovich[9], T. Kluge[9], G. Knies[9], A. Knutsson[19], V. Korbel[9], P. Kostka[38], K. Krastev[9], J. Kretzschmar[38], A. Kropivnitskaya[24], K. Krüger[13], M.P.J. Landon[18], W. Lange[38], T. Laštovička[38,32], G. Laštovička-Medin[30], P. Laycock[17], A. Lebedev[25], G. Leibenguth[39], V. Lendermann[13], S. Levonian[9], L. Lindfeld[40], K. Lipka[38], A. Liptaj[26], B. List[39], J. List[10], E. Lobodzinska[38,5], N. Loktionova[25], R. Lopez-Fernandez[23], V. Lubimov[24], A.-I. Lucaci-Timoce[9], H. Lueders[10], D. Lüke[6,9], T. Lux[10], L. Lytkin[11], A. Makankine[7], N. Malden[20], E. Malinovski[25], S. Mangano[39], P. Marage[3], R. Marshall[20], M. Martisikova[9], H.-U. Martyn[1], S.J. Maxfield[17], A. Mehta[17], K. Meier[13], A.B. Meyer[9], H. Meyer[36], J. Meyer[9], V. Michels[9], S. Mikocki[5], I. Milcewicz-Mika[5], D. Milstead[17], D. Mladenov[34], A. Mohamed[17], F. Moreau[28], A. Morozov[7], J.V. Morris[4], M.U. Mozer[12], K. Müller[40], P. Murín[15,43], K. Nankov[34], B. Naroska[10], Th. Naumann[38], P.R. Newman[2], C. Niebuhr[9], A. Nikiforov[26], G. Nowak[5], K. Nowak[40], M. Nozicka[32], R. Oganezov[37], B. Olivier[26], J.E. Olsson[9], S. Osman[19], D. Ozerov[24], V. Palichik[7], I. Panagoulias[9], T. Papadopoulou[9], C. Pascaud[27], G.D. Patel[17], H. Peng[9], E. Perez[8], D. Perez-Astudillo[22], A. Perieanu[9], A. Petrukhin[24], D. Pitzl[9], R. Plačakytė[26], B. Portheault[27], B. Povh[11], P. Prideaux[17], A.J. Rahmat[17], N. Raicevic[30], P. Reimer[31], A. Rimmer[17], C. Risler[9], E. Rizvi[18], P. Robmann[40], B. Roland[3], R. Roosen[3], A. Rostovtsev[24], Z. Rurikova[26], S. Rusakov[25], F. Salvaire[10], D.P.C. Sankey[4], E. Sauvan[21], S. Schätzel[9], S. Schmidt[9], S. Schmitt[9], C. Schmitz[40], L. Schoeffel[8], A. Schöning[39], H.-C. Schultz-Coulon[13], F. Sefkow[9], R.N. Shaw-West[2], I. Sheviakov[25], L.N. Shtarkov[25], T. Sloan[16], P. Smirnov[25], Y. Soloviev[25], D. South[9], V. Spaskov[7], A. Specka[28], M. Steder[9], B. Stella[33], J. Stiewe[13], U. Straumann[40], D. Sunar[3], V. Tchoulakov[7], G. Thompson[18], P.D. Thompson[2], T. Toll[9], F. Tomasz[15], D. Traynor[18], P. Truöl[40], I. Tsakov[34], G. Tsipolitis[9,41], I. Tsurin[9], J. Turnau[5], E. Tzamariudaki[26], K. Urban[13], M. Urban[40], A. Usik[25], D. Utkin[24], A. Valkárová[32], C. Vallée[21], P. Van Mechelen[3], A. Vargas Trevino[6], Y. Vazdik[25], C. Veelken[17], S. Vinokurova[9], V. Volchinski[37], K. Wacker[6], G. Weber[10], R. Weber[39], D. Wegener[6],

C. Werner[12], M. Wessels[9], B. Wessling[9], Ch. Wissing[6], R. Wolf[12], E. Wünsch[9], S. Xella[40], W. Yan[9], V. Yeganov[37], J. Žáček[32], J. Zálešák[31], Z. Zhang[27], A. Zhelezov[24], A. Zhokin[24], Y.C. Zhu[9], J. Zimmermann[26], T. Zimmermann[39], H. Zohrabyan[37], and F. Zomer[27]

[1] *I. Physikalisches Institut der RWTH, Aachen, Germany*[a]
[2] *School of Physics and Astronomy, University of Birmingham, Birmingham, UK*[b]
[3] *Inter-University Institute for High Energies ULB-VUB, Brussels; Universiteit Antwerpen, Antwerpen; Belgium*[c]
[4] *Rutherford Appleton Laboratory, Chilton, Didcot, UK*[b]
[5] *Institute for Nuclear Physics, Cracow, Poland*[d]
[6] *Institut für Physik, Universität Dortmund, Dortmund, Germany*[a]
[7] *Joint Institute for Nuclear Research, Dubna, Russia*
[8] *CEA, DSM/DAPNIA, CE-Saclay, Gif-sur-Yvette, France*
[9] *DESY, Hamburg, Germany*
[10] *Institut für Experimentalphysik, Universität Hamburg, Hamburg, Germany*[a]
[11] *Max-Planck-Institut für Kernphysik, Heidelberg, Germany*
[12] *Physikalisches Institut, Universität Heidelberg, Heidelberg, Germany*[a]
[13] *Kirchhoff-Institut für Physik, Universität Heidelberg, Heidelberg, Germany*[a]
[14] *Institut für Experimentelle und Angewandte Physik, Universität Kiel, Kiel, Germany*
[15] *Institute of Experimental Physics, Slovak Academy of Sciences, Košice, Slovak Republic*[f]
[16] *Department of Physics, University of Lancaster, Lancaster, UK*[b]
[17] *Department of Physics, University of Liverpool, Liverpool, UK*[b]
[18] *Queen Mary and Westfield College, London, UK*[b]
[19] *Physics Department, University of Lund, Lund, Sweden*[g]
[20] *Physics Department, University of Manchester, Manchester, UK*[b]
[21] *CPPM, CNRS/IN2P3 - Univ. Mediterranee, Marseille - France*
[22] *Departamento de Fisica Aplicada, CINVESTAV, Mérida, Yucatán, México*[j]
[23] *Departamento de Fisica, CINVESTAV, México*[j]
[24] *Institute for Theoretical and Experimental Physics, Moscow, Russia*[k]
[25] *Lebedev Physical Institute, Moscow, Russia*[e]
[26] *Max-Planck-Institut für Physik, München, Germany*
[27] *LAL, Université de Paris-Sud, IN2P3-CNRS, Orsay, France*
[28] *LLR, Ecole Polytechnique, IN2P3-CNRS, Palaiseau, France*
[29] *LPNHE, Universités Paris VI and VII, IN2P3-CNRS, Paris, France*
[30] *Faculty of Science, University of Montenegro, Podgorica, Serbia and Montenegro*[e]
[31] *Institute of Physics, Academy of Sciences of the Czech Republic, Praha, Czech Republic*[h]
[32] *Faculty of Mathematics and Physics, Charles University, Praha, Czech Republic*[h]
[33] *Dipartimento di Fisica Università di Roma Tre and INFN Roma 3, Roma, Italy*
[34] *Institute for Nuclear Research and Nuclear Energy, Sofia, Bulgaria*[e]
[35] *Paul Scherrer Institut, Villigen, Switzerland*
[36] *Fachbereich C, Universität Wuppertal, Wuppertal, Germany*
[37] *Yerevan Physics Institute, Yerevan, Armenia*
[38] *DESY, Zeuthen, Germany*
[39] *Institut für Teilchenphysik, ETH, Zürich, Switzerland*[i]
[40] *Physik-Institut der Universität Zürich, Zürich, Switzerland*[i]

[41] *Also at Physics Department, National Technical University, Zografou Campus, GR-15773 Athens, Greece*
[42] *Also at Rechenzentrum, Universität Wuppertal, Wuppertal, Germany*
[43] *Also at University of P.J. Šafárik, Košice, Slovak Republic*
[44] *Also at CERN, Geneva, Switzerland*
[45] *Also at Max-Planck-Institut für Physik, München, Germany*
[46] *Also at Comenius University, Bratislava, Slovak Republic*

[†] *Deceased*

[a] *Supported by the Bundesministerium für Bildung und Forschung, FRG, under contract numbers 05 H1 1GUA /1, 05 H1 1PAA /1, 05 H1 1PAB /9, 05 H1 1PEA /6, 05 H1 1VHA /7 and 05 H1 1VHB /5*
[b] *Supported by the UK Particle Physics and Astronomy Research Council, and formerly by the UK Science and Engineering Research Council*
[c] *Supported by FNRS-FWO-Vlaanderen, IISN-IIKW and IWT and by Interuniversity Attraction Poles Programme, Belgian Science Policy*
[d] *Partially Supported by the Polish State Committee for Scientific Research, SPUB/DESY/P003/DZ 118/2003/2005*
[e] *Supported by the Deutsche Forschungsgemeinschaft*
[f] *Supported by VEGA SR grant no. 2/4067/ 24*
[g] *Supported by the Swedish Natural Science Research Council*
[h] *Supported by the Ministry of Education of the Czech Republic under the projects LC527 and INGO-1P05LA259*
[i] *Supported by the Swiss National Science Foundation*
[j] *Supported by CONACYT, México, grant 400073-F*
[k] *Partially Supported by Russian Foundation for Basic Research, grants 03-02-17291 and 04-02-16445*

# 1 Introduction

Diffractive vector meson production in $ep$ interactions with large negative four-momentum transfer squared at the proton vertex, $t$, provides a powerful means to probe the nature of the diffractive exchange. It has been proposed as a process in which Quantum Chromodynamics (QCD) effects predicted by the BFKL evolution equation [1, 2] could be observed. Theoretically, the large momentum transfer provides the hard scale necessary for the application of perturbative QCD (pQCD) models. In such models, diffractive vector meson production is viewed, in the proton rest frame, as a sequence of three processes well separated in time: the intermediate photon fluctuates into a $q\bar{q}$ pair; the $q\bar{q}$ pair is involved in a hard interaction with the proton via the exchange of a colour singlet state, and the $q\bar{q}$ pair recombines to form a vector meson. At leading order (LO), the interaction between the $q\bar{q}$ pair and the proton is represented by the exchange of two gluons. Beyond LO, the exchange of a gluon ladder has to be considered which, in the leading logarithm (LL) approximation, can be described by the BFKL equation. The treatment of the formation of the vector meson, which is a non-perturbative process, involves a parameterisation of the meson wavefunction.

At high $|t|$, the $t$ dependence of vector meson production and of the spin density matrix elements has been measured in photoproduction by ZEUS [3] ($\rho$, $\phi$, $J/\psi$) and H1 [4,5] ($J/\psi$, $\psi(2s)$). H1 has also measured the $t$ dependence of the spin density matrix elements for the $\rho$ meson at high $|t|$ in electroproduction [6]. The data on light vector meson production ($\rho$, $\phi$) at large $|t|$ indicate a violation of $s$-channel helicity conservation (SCHC), i.e. the non-conservation of the helicity between the exchanged photon and the vector meson. This is in contrast to measurements of the heavier $J/\psi$ meson, where $s$-channel helicity is seen to be conserved [3, 4].

This paper presents new measurements of the diffractive production of $\rho$ mesons at large $|t|$, in the range $1.5 < |t| < 10\ \mathrm{GeV}^2$:

$$ep \to e\rho Y; \rho \to \pi^+\pi^-, \tag{1}$$

in the photoproduction regime, i.e. $Q^2 \simeq 0\ \mathrm{GeV}^2$ where $Q^2$ is the modulus of the squared four momentum carried by the intermediate photon. The system $Y$ represents either an elastically scattered proton or a low mass dissociated system. A clean signature and low background rates make this process experimentally attractive and it is possible to precisely determine the kinematics of the process through an accurate measurement of the vector meson four momentum. The dependence on $t$ of the cross section is measured and the spin density matrix elements are extracted, which provide information on the helicity structure of the interaction.

# 2 Perturbative QCD Models

Perturbative QCD calculations at leading order (two-gluon exchange) have been performed for high $|t|$ vector meson photoproduction in [7]. For light vector mesons, these calculations indicate that, although the initial photon is transversely polarised, the vector meson is produced predominantly in a longitudinal state. Intuitively, this can be understood as follows. Since the light quark and antiquark have opposite helicities (chiral-even configuration), the pair must be in an orbital momentum state with projection $L_z = \pm 1$ onto the photon axis, in order to conserve the photon spin projection. The hard interaction between the dipole and the gluon system does not affect the dipole size nor the quark and antiquark helicities, but modifies the dipole line of flight. This implies a damping by a factor $\propto 1/|t|$ of the probability of measuring the value $L_z = \pm 1$ for the projection of the dipole angular momentum onto its line of flight, and hence of transversely polarised vector meson production.

However, in contrast to these pQCD expectations, experimental observations indicate that light vector mesons are produced predominantly in a transverse polarisation state [3]. As first realised in [8] an enhanced production of transversely polarised $\rho$ mesons can be accounted for by the possibility for a real photon to couple to a $q\bar{q}$ pair in a chiral-odd spin configuration even in the case of light quarks[1].

The data presented in this paper are compared to two theoretical predictions: a fixed order calculation in which the hard interaction is approximated by the exchange of two gluons[2], and a LL calculation in which it is described according to the BFKL evolution. In both cases, the chiral-odd component of the photon wavefunction is obtained by giving the quarks a "constituent quark mass" $m = m_V/2$, where $m_V$ is the mass of the vector meson, and a set of QCD light-cone wavefunctions for the vector meson [11] is used.

The BFKL calculation is described in [9, 10]. The BFKL resummation cures some possible instabilities which might affect the two-gluon predictions [1]. The expansions on the light-cone of the relevant hadronic matrix elements are performed up to twist-3, i.e. next-to-leading twist. The leading logarithm nature of the calculation prevents an absolute prediction for the normalisation of the cross sections, due to the presence of an undefined energy scale $\Lambda$. In [9, 10] this scale is allowed to run with $t$ according to $\Lambda^2 = m_V^2 - \gamma t$, where $\gamma$ is a free parameter. The value of the strong coupling constant is fixed since this is appropriate in the LL approximation and has proved successful [12, 13] in describing previous data. The parameter values, as obtained from a fit to the ZEUS data in [3], are: $\gamma = 1.0$ and $\alpha_s^{BFKL} = 0.20$ [14].

# 3 Data Analysis

## 3.1 Event Selection

The data used for the present analysis were taken with the H1 detector in the year 2000 and correspond to an integrated luminosity of $20.1\ \mathrm{pb}^{-1}$. In this period, the energies of the HERA

[1]Note that in the case of heavy vector mesons, the relevant non-relativistic wavefunction, with equal sharing of the photon longitudinal momentum by the two heavy quarks, ensures that the amplitude for producing a longitudinally polarised meson vanishes. Only the chiral-odd amplitude, which is naturally present due to the non-zero quark mass, remains. Hence heavy vector mesons are expected to be transversely polarised, as confirmed by the experimental observations.

[2]The two-gluon model predictions for the kinematic region considered here were provided by the authors of [9, 10]. The model differs from that proposed in [8] in the way the chiral-odd configurations are introduced.

proton and positron beams were 920 GeV and 27.5 GeV, respectively. The kinematic domain of the measurement is:

$$\begin{array}{rcl} & Q^2 & < 0.01\ \mathrm{GeV}^2 \\ 75 < & W & < 95\ \mathrm{GeV} \\ 1.5 < & |t| & < 10\ \mathrm{GeV}^2 \\ & M_Y & < 5\ \mathrm{GeV} \end{array} \tag{2}$$

where $W$ is the photon-proton centre of mass energy and $M_Y$ is the mass of the proton remnant system.

The relevant parts of the detector, for which more details can be found in [15], are the central tracking detector (which covers the polar angular range $20^\circ < \theta < 160^\circ$), the liquid argon (LAr) calorimeter (which covers the polar angular range $4^\circ < \theta < 154^\circ$) and an electron tagger located at $44$ m from the interaction point, which detects the scattered positron at a small angle to the backward direction[3]. The $44$ m electron tagger is a $2 \times 3$ array of Čerenkov crystal calorimeters used to select photoproduction events in the range $Q^2 < 0.01\ \mathrm{GeV}^2$. The trigger system used in this analysis selects events with an energy deposit greater than $10$ GeV in the $44$ m electron tagger, at least one charged track with a transverse momentum above $400$ MeV in the central tracker and a reconstructed interaction vertex. Additionally, there is a veto on the amount of energy deposited in the forward region of the LAr.

Events corresponding to reaction (1), in the kinematic range defined by relations (2), are selected by requesting:

- the reconstruction of an energy deposit of more than 15 $\mathrm{GeV}$ in the $44$ m electron tagger (the scattered positron candidate);
- the reconstruction in the central tracking detector of the trajectories of exactly two oppositely charged particles (pion candidates) with transverse momenta larger than $150$ MeV and polar angles within $20^\circ < \theta < 155^\circ$. In order to ensure a well understood trigger efficiency, at least one track is required to have a transverse momentum above $450$ MeV;
- the absence of any localised energy deposit larger than 400 MeV in the LAr calorimeter which is not associated with either of the two reconstructed tracks. This cut reduces backgrounds due to the diffractive production of systems decaying into two charged and additional neutral particles. Further, it limits the mass of the proton dissociative system to $M_Y \lesssim 5$ GeV which ensures that the events lie within the diffractive regime $M_Y \ll W$. Restricting the analysis to low values of $M_Y$ also reduces the uncertainties arising from the parametrisation of the $M_Y$ dependence of the cross section;
- events in the mass range $0.6 < M_{\pi\pi} < 1.1$ GeV and discarding events with $M_{KK} < 1.04$ GeV, where $M_{\pi\pi}$ and $M_{KK}$ are the invariant masses of the two selected tracks when considered as pions or kaons respectively (no explicit hadron identification is performed for this analysis). The latter cut reduces the background due to diffractive production of $\phi$ mesons.

[3]In the H1 convention, the $z$ axis is defined by the colliding beams, the forward direction being that of the outgoing proton beam and the backward direction that of the positron beam. Transverse and longitudinal momenta are defined with respect to the proton beam direction.

The final sample consists of 2628 events. Further details of this analysis may be found in [16].

### 3.2 Kinematics and Helicity Structure

The three momentum of the $\rho$ meson is computed as the sum of the two charged pion candidate momenta. The variable $W$ is reconstructed from the $\rho$ meson, rather than from the energy of the scattered positron candidate which is less precisely measured by the electron tagger, using the Jacquet-Blondel method [17]:

$$W^2 \simeq 2E_p(E_\rho - p_{z,\rho}) \tag{3}$$

where $E_p$ is the energy of the incoming proton and $E_\rho$ and $p_{z,\rho}$ are the energy and longitudinal momentum of the $\rho$ meson, respectively. In the photoproduction regime, the variable $t$ is well approximated by the negative transverse momentum squared of the $\rho$ meson, $t \simeq -p_{t,\rho}^2$.

The measurement of the production and decay angular distributions provides information on the helicity structure of the interaction. Three angles are defined [18] as illustrated in Fig. 1: $\Phi$ is the angle between the $\rho$ production plane (defined as the plane containing the virtual photon and the $\rho$ meson) and the positron scattering plane in the $\gamma p$ centre of mass system; $\theta^*$ is the polar angle of the positively charged decay pion in the $\rho$ rest frame with respect to the meson direction as defined in the $\gamma p$ centre of mass frame and $\phi^*$ is its azimuthal angle relative to the $\rho$ production plane.

In this paper, the distributions of the angles $\phi^*$ and $\theta^*$ are analysed (the angle $\Phi$ is not accessible in photoproduction) giving access to the spin density matrix elements $r_{00}^{04}$, $\mathrm{Re}\,[r_{10}^{04}]$ and $r_{1-1}^{04}$ [19]. For a $\rho$ meson decaying into two pions, the normalised two-dimensional angular distribution [19], averaged over $\Phi$, is

$$\begin{aligned} \frac{1}{\sigma}\frac{\mathrm{d}^2\sigma}{\mathrm{d}\cos\theta^*\mathrm{d}\phi^*} &= \frac{3}{4\pi}\left[\frac{1}{2}(1-r_{00}^{04}) + \frac{1}{2}(3r_{00}^{04}-1)\cos^2\theta^* \right. \\ &\left. -\sqrt{2}\mathrm{Re}\left[r_{10}^{04}\right]\sin 2\theta^*\cos\phi^* - r_{1-1}^{04}\sin^2\theta^*\cos 2\phi^*\right]. \end{aligned} \tag{4}$$

Integrating over $\cos\theta^*$ or $\phi^*$ further reduces this distribution to the one dimensional distributions

$$\frac{\mathrm{d}\sigma}{\mathrm{d}\cos\theta^*} \propto 1 - r_{00}^{04} + (3r_{00}^{04}-1)\cos^2\theta^* \tag{5}$$

and

$$\frac{\mathrm{d}\sigma}{\mathrm{d}\phi^*} \propto 1 - 2r_{1-1}^{04}\cos 2\phi^*. \tag{6}$$

The spin density matrix elements are defined as bilinear combinations of the helicity amplitudes $M_{\lambda_\gamma\lambda_V}$, where $\lambda_\gamma, \lambda_V = -, 0, +$ are the respective helicities of the photon and the vector meson. For photoproduction, where the photon is quasi-real, the longitudinal photon polarisation component is negligible and only the transverse polarisation states remain. The photon-meson transitions can thus be described in terms of three independent helicity amplitudes $M_{++}$, $M_{+0}$,

$M_{+-}$[4], which correspond to no change in helicity (no-flip), a single change in helicity (single-flip) and a double change in helicity (double-flip), respectively. In this case, the matrix elements are related to the helicity amplitudes by

$$r^{04}_{00} = \frac{|M_{+0}|^2}{|M_{++}|^2 + |M_{+0}|^2 + |M_{+-}|^2} \tag{7}$$

$$r^{04}_{10} = \frac{1}{2}\frac{M_{++}M^*_{+0} - M_{+-}M^*_{+0}}{|M_{++}|^2 + |M_{+0}|^2 + |M_{+-}|^2} \tag{8}$$

$$r^{04}_{1-1} = \frac{1}{2}\frac{M_{++}M^*_{+-} + M_{+-}M^*_{++}}{|M_{++}|^2 + |M_{+0}|^2 + |M_{+-}|^2}. \tag{9}$$

Under $s$-channel helicity conservation, only the amplitude $M_{++}$ is non-zero and consequently the $r^{04}_{00}$, $r^{04}_{10}$ and $r^{04}_{1-1}$ matrix elements should all be zero. In contrast, both the BFKL and two-gluon models predict a violation of SCHC. In the case of the LL BFKL model, the helicity amplitudes are predicted to follow a hierarchical structure with $|M_{++}| > |M_{+-}| > |M_{+0}|$ [9, 10].

### 3.3 Monte Carlo Simulation

A Monte Carlo simulation based on the DIFFVM program [20] is used to describe the diffractive production and decay of $\rho$ mesons, and to correct the data for acceptance, efficiency and smearing effects. The $Q^2$ and $W$ dependences of the cross section are taken from previous measurements [21]. The $t$ dependence is taken according to the power law measured in the present analysis following an iterative procedure. The simulation includes the angular distributions corresponding to the measurements of the present analysis for the $r^{04}_{00}$, $r^{04}_{1-1}$ and the $\mathrm{Re}\,[r^{04}_{10}]$ matrix elements. The $M_Y$ spectrum is parameterised as $\mathrm{d}\sigma/\mathrm{d}M_Y^2 \propto f(M_Y^2)/M_Y^{2.15}$ [22], where $f(M_Y^2) = 1$ for $M_Y^2 > 3.6$ GeV$^2$ and, at lower masses, is a function which accounts for the production of excited nucleon states. Other angular distributions and correlations are taken in the $s$-channel helicity conservation approximation. The mass distribution is described by a relativistic Breit-Wigner distribution, the mass and the width of the $\rho$ being fixed [23], including skewing effects resulting from the interference with open pion pair production [24, 25] taken from the current analysis. For studies of systematics uncertainties, all simulation parameters have been varied within errors (see section 3.5).

The DIFFVM simulation is also used for the description of the $\omega$, $\phi$ and $\rho'$ backgrounds (see next section). Here the $t$ distributions are described using the same parameterisation as for the $\rho$ meson and the angular distributions are kept in the SCHC approximation, which is justified by the smallness of these contributions.

All generated samples are passed through a detailed simulation of the detector response based on the GEANT3 program [26], and through the same reconstruction software as used for the data. Figure 2 presents the observed and simulated distributions for several variables of the selected sample of events. The simulated distributions, which include the amounts of background

[4]The three corresponding amplitudes $M_{--}$, $M_{-0}$ and $M_{-+}$ are not independent since they satisfy $M_{++} = M_{--}$, $M_{+-} = M_{-+}$ and $M_{+0} = -M_{-0}$ due to parity symmetry.

discussed in section 3.4, are normalised to the number of observed events. Reasonable agreement is observed for all distributions, showing that the Monte-Carlo simulations can reliably be used to correct the data for acceptance and smearing effects. The structure in the $\phi^*$ distribution (Fig. 2f) is due to the low geometrical acceptance of the central tracking detector in the case where the angle between the $\rho$ meson production and decay planes is small ($\phi^* \sim 0°$ or $180°$), which leads to the emission of one of the pions at a small angle relative to the beam direction.

## 3.4 Backgrounds

Diffractive photoproduction of $\omega$, $\phi$ and $\rho'$ mesons[5] can fake $\rho$ production through the decay channels:

$$\begin{aligned} &\omega \to \pi^+\pi^-\pi^0, \\ &\phi \to \pi^+\pi^-\pi^0, \quad \phi \to K^0_S K^0_L, \\ &\rho' \to \rho^\pm\pi^\mp\pi^0, \quad \rho^\pm \to \pi^\pm\pi^0, \end{aligned} \tag{10}$$

if the decay photons of the $\pi^0$ or the $K^0_L$ mesons are not detected[6]. This happens in the cases where the energy of the neutral particle is deposited in an inactive region of the detector, is associated to the charged pion tracks, or is below the noise threshold. Diffractive photoproduction of $\omega$ and $\phi$ mesons also gives the same topology as that of the $\rho$ meson within the detector through the decay channels

$$\begin{aligned} \omega &\to \pi^+\pi^-, \\ \phi &\to K^+K^-. \end{aligned} \tag{11}$$

To estimate the corresponding backgrounds, the $\omega$, $\phi$ and $\rho'$ cross sections were taken from measured ratios to the $\rho$ cross section in the $Q^2$ range relevant for the analysis: $\sigma_\omega \ / \ \sigma_\rho = 0.106 \pm 0.019$ [27], $\sigma_\phi \ / \ \sigma_\rho = 0.156^{+0.029}_{-0.019}$ [3] and $\sigma(\rho' \to \rho^\pm\pi^\mp\pi^0) \ / \ \sigma_\rho = 0.2 \pm 0.1$. In the latter case, the ratio is obtained from the ratio $\sigma(\rho' \to \rho^0\pi^+\pi^-) \ / \ \sigma_\rho = 0.10 \pm 0.05$, measured in electron [28] and muon [29] scattering off a liquid hydrogen target, under the assumption

$$\frac{\sigma(\rho' \to \rho^+\pi^-\pi^0) + \sigma(\rho' \to \rho^-\pi^+\pi^0)}{\sigma(\rho' \to \rho^0\pi^+\pi^-)} = 2. \tag{12}$$

The background contributions in the selected kinematic domain (2) and for the selected $\rho$ mass range are estimated and subtracted separately for each measurement interval using the Monte Carlo simulations. In total, the backgrounds amount to 0.5%, 0.2% and 1.2% for $\omega$, $\phi$ and $\rho'$ production, respectively.

[5]The detailed structure [23] of the $\rho'$ state is not relevant for the present study. The name $\rho'$ is, therefore, used to represent both the $\rho'(1450)$ and the $\rho'(1700)$. In the DIFFVM simulation, the $\rho'$ mass and width are taken as 1450 MeV and 300 MeV, respectively.

[6]The contribution from background processes leading to more than two charged particles in the final state is negligible.

### 3.5 Systematic Uncertainties

The systematic uncertainties on the measurements are estimated by varying the event selection, the parameters of the $\rho$ Monte Carlo simulation and the properties of subtracted backgrounds. The following sources of systematic error are taken into account:

- **Uncertainties in the $\rho$ simulation**
  The uncertainty on the input $t$ distribution, used to compute acceptances and smearing effects and to adjust the measurements to the mean $t$ value for each $t$ interval, is taken into account by varying the exponent of the Monte Carlo power law by $\pm 0.5$. The uncertainty in the modelling of the dissociative proton system $Y$ is estimated by reweighting the proton remnant mass distribution by factors $(1/M_Y^2)^{\pm 0.3}$ [22]. For the angular distributions, the spin density matrix elements are varied around the values measured in the current data according to the spread of the observed results with $t$ by $\pm\ 0.03$ for $r_{00}^{04}$, $\pm\ 0.02$ for $\mathrm{Re}\,[r_{10}^{04}]$ and ${}^{+0.02}_{-0.04}$ for $r_{1-1}^{04}$. Finally, in the low $|t|$ region where non-zero skewing is observed in the $\rho$ line shape, the skewing parameter is varied according to the uncertainty of the fit to the invariant mass distribution (see section 4).

- **Uncertainties on the background distributions**
  The amount of background is varied by changing the ratio of the background cross sections to the $\rho$ cross section according to their uncertainties, as quoted in section 3.4. The $t$ dependence of the $\rho'$ distribution, which provides the largest background contribution, is further varied using weighting factors of $(1/|t|)^{\pm 2.0}$.

- **Uncertainties in the detector description**
  Uncertainties on the detailed $p_t$ and angular dependences of the trigger efficiencies are taken into account by varying them within their estimated errors. The uncertainty on the tracking acceptance at large angles is estimated by varying the cut on the polar angle of the reconstructed tracks between $150^\circ$ and $160^\circ$. The threshold for the detection of energy deposits in the LAr that are not associated to the two pion candidates is varied between $300$ MeV and $500$ MeV. Finally, the influence of the uncertainty in the description of the electron tagger acceptance is estimated by shifting the acceptance range in $W$ by 3%.

For the measurement of the $t$ dependence, the largest sources of systematic uncertainty are the slope of the $t$ distribution in the MC, the variation of the LAr energy threshold and the variation of the upper $\theta$ cut. Additionally, for the measurement of the spin density matrix elements, the parameterisation of the matrix elements in the MC provides a significant effect. For each contribution, the relative effect on the extracted $t$ slope is less than $\pm 1\%$, and the effect on the measured spin density matrix elements is less than $\pm 0.015$.

The total systematic error on the cross section is obtained by adding the individual contributions, which are considered as uncorrelated, in quadrature. Correlated systematics which affect only the normalisation cancel since only normalised cross sections are presented here. For the extraction of the $t$ slope and the spin density matrix elements, the systematic error is obtained by repeating the appropriate fit after shifting the data points according to each individual systematic uncertainty. Again, the individual contributions are added in quadrature.

# 4 Results

In each bin of the kinematic variables, the cross section is computed from the number of events in the bin, fully corrected for backgrounds, acceptance and smearing effects using the Monte Carlo simulations described above. At low $|t|$, the data are further corrected for the skewing effect obtained from a fit to the present data using the Ross-Stodolsky [25] parameterisation in which the mass and the width of the $\rho$ are fixed [23]. This correction amounts to $2.6\%$ for $1.5 < |t| < 2.2$ GeV$^2$. At higher $|t|$, the skewing effect is negligible. All cross sections presented below, as well as the theoretical model predictions, are normalised to their integrals in the respective kinematic domain.

## 4.1 Dependence on $t$

The $t$ dependence of the $ep \to e\rho Y$ cross section is presented in Fig. 3 and table 1. The data are plotted at the mean value in each $t$ interval determined according to the parameterisation of the $t$ dependence. The data are well described over the measured range of $t$ by a power law dependence of the form $\mathrm{d}\sigma/\mathrm{d}|t| \propto |t|^{-n}$ where $n = 4.26 \pm 0.06\ (\mathrm{stat.})\ ^{+0.06}_{-0.04}\ (\mathrm{syst.})$, as determined by a $\chi^2$ minimisation. An exponential parameterisation of the form $\mathrm{d}\sigma/\mathrm{d}|t| \propto e^{-b|t|}$ is unable to describe the data over the full $t$ range. The data in Fig. 3 are compared with the predictions of the two-gluon model both with fixed and running $\alpha_s$ and with those of the BFKL model [9, 10]. The BFKL model provides a reasonable description of the $t$ dependence, in contrast to the two-gluon model predictions.

The ZEUS Collaboration has previously published data on the diffractive photoproduction of $\rho$ mesons with proton dissociation in the range $1.1 < |t| < 10.0$ GeV$^2$ [3] and observes a power law with exponent $n = 3.21 \pm 0.04\ (\mathrm{stat.}) \pm 0.15\ (\mathrm{syst.})$. This is significantly shallower than the result obtained here. The difference in slope can be understood in terms of the difference in the kinematic region over which the two measurements are made, in particular the maximum value of $M_Y$: the phase space of the ZEUS measurement corresponds to $M_Y < 12$ GeV (31 GeV) at $|t| = 1.5$ GeV$^2$ ($|t| = 10$ GeV$^2$) whereas the phase space of this measurement is $M_Y < 5$ GeV. Both measurements are well described by the BFKL model using similar parameters [10, 14].

## 4.2 Spin Density Matrix Elements

The spin density matrix elements are extracted by a two-dimensional likelihood fit of equation (4) to the data. The normalised single differential distributions in $\cos\theta^*$ and $\phi^*$ are shown in Fig. 4 for three ranges of $t$. The solid curves show the projection of the two-dimensional fit and the dashed curves show the expectation of $s$-channel helicity conservation. A flat $\phi^*$ behaviour is clearly disfavoured, indicating a violation of SCHC. The values of the three extracted matrix elements are shown in Fig. 5 and table 2 as a function of $|t|$. Within the experimental uncertainty, no strong dependence on $t$ is observed. Measurements of the spin density matrix elements for the photoproduction of $\rho$ mesons obtained by the ZEUS Collaboration [3] are also shown. There is a reasonable agreement between the results of the two experiments.

| $\lvert t\rvert$ range ($\mathrm{GeV}^2$) | $\langle\lvert t\rvert\rangle$ ($\mathrm{GeV}^2$) | $1/\sigma\ \mathrm{d}\sigma/\mathrm{d}\lvert t\rvert$ ($\mathrm{GeV}^{-2}$) |
|---|---|---|
| $1.5 - 2.0$ | $1.72$ | $1.176 \pm 0.032\ ^{+0.020}_{-0.012}$ |
| $2.0 - 2.5$ | $2.23$ | $0.447 \pm 0.019\ ^{+0.0051}_{-0.018}$ |
| $2.5 - 3.0$ | $2.73$ | $0.183 \pm 0.012\ ^{+0.0072}_{-0.0062}$ |
| $3.0 - 3.5$ | $3.23$ | $0.0850 \pm 0.0076\ ^{+0.0025}_{-0.0041}$ |
| $3.5 - 4.0$ | $3.74$ | $0.0401 \pm 0.0051\ ^{+0.0031}_{-0.0019}$ |
| $4.0 - 5.0$ | $4.45$ | $0.0188 \pm 0.0025\ ^{+0.0014}_{-0.0009}$ |
| $5.0 - 6.0$ | $5.46$ | $0.00848 \pm 0.00167\ ^{+0.00066}_{-0.00034}$ |
| $6.0 - 10.0$ | $7.56$ | $0.00185 \pm 0.00039\ ^{+0.00011}_{-0.00009}$ |

Table 1: The normalised differential cross section for $ep \to e\rho Y$ as a function of $t$. The first errors are statistical and the second are systematic. The kinematic range of the measurement is given in (2).

The small values of $r^{04}_{00}$, which is directly proportional to the square of the single-flip helicity amplitude $M_{+0}$, signify that the probability of producing a longitudinally polarised $\rho$ from a transversely polarised photon is low, varying from $(4 \pm 2)\%$ at $|t| = 1.79\ \mathrm{GeV}^2$ to $(6 \pm 6)\%$ at $|t| = 4.69\ \mathrm{GeV}^2$. The non-zero values of $\mathrm{Re}\,[r^{04}_{10}]$ confirm that, although small, a single-flip contribution is present. The production of transversely polarised $\rho$ mesons must, therefore, dominate and the finite negative values of $r^{04}_{1-1}$ show clear evidence for a helicity double-flip contribution. Both these observations indicate a violation of the SCHC hypothesis. This is in contrast with the results on the $J/\psi$ meson, where, within experimental errors, the measured spin density matrix elements [3,4] are all compatible with zero.

The two-gluon model predictions (dotted lines in Fig. 5) [9, 10] are unable to describe the measured spin density matrix elements. In particular, the model predicts too high values of $r^{04}_{00}$, i.e. too high probabilities for producing longitudinally polarised $\rho$ mesons. For the BFKL predictions [9, 10], which are shown by the full lines in Fig. 5, $r^{04}_{00}$ is well described but the prediction for $r^{04}_{1-1}$ is too negative and the wrong sign for $\mathrm{Re}\,[r^{04}_{10}]$ is predicted. The inability to describe the $\mathrm{Re}\,[r^{04}_{10}]$ matrix element is the major obstacle for the BFKL model.

# 5 Summary

The diffractive photoproduction of $\rho$ mesons, $ep \to e\rho Y$, has been studied using the H1 detector at HERA in the kinematic range $Q^2 < 0.01\ \mathrm{GeV}^2$, $75 < W < 95$ GeV, $1.5 < |t| < 10\ \mathrm{GeV}^2$ and $M_Y < 5$ GeV. The $t$ dependence of the cross section is measured and fitted with a power law of the form $|t|^{-n}$, which fits the data well and results in $n = 4.26 \pm 0.06\,(\mathrm{stat.})\ ^{+0.06}_{-0.04}\,(\mathrm{syst.})$. It is reasonably described by a BFKL-based model, while both two-gluon predictions considered here, with different treatments of the strong coupling, fail to describe the data.

| $\lvert t\rvert$ range (GeV$^2$) | $\langle \lvert t\rvert \rangle$ (GeV$^2$) | $r^{04}_{00}$ | $\mathrm{Re}\,[r^{04}_{10}]$ | $r^{04}_{1-1}$ |
|---|---|---|---|---|
| $1.5 - 2.2$ | $1.79$ | $0.038 \pm 0.017\,^{+0.011}_{-0.012}$ | $0.064 \pm 0.012\,^{+0.005}_{-0.015}$ | $-0.088 \pm 0.015\,^{+0.007}_{-0.014}$ |
| $2.2 - 3.5$ | $2.64$ | $0.029 \pm 0.025\,^{+0.010}_{-0.013}$ | $0.031 \pm 0.019\,^{+0.007}_{-0.011}$ | $-0.138 \pm 0.021\,^{+0.011}_{-0.011}$ |
| $3.5 - 10.0$ | $4.69$ | $0.062 \pm 0.058\,^{+0.015}_{-0.012}$ | $0.057 \pm 0.034\,^{+0.004}_{-0.007}$ | $-0.119 \pm 0.044\,^{+0.011}_{-0.009}$ |

Table 2: The three spin density matrix elements $r^{04}_{00}$, $r^{04}_{1-1}$ and $\mathrm{Re}\,[r^{04}_{10}]$ for $\rho$ meson photoproduction as a function of $|t|$. The first errors are statistical and the second are systematic.

The spin density matrix elements $r^{04}_{00}$, $r^{04}_{1-1}$ and $\mathrm{Re}\,[r^{04}_{10}]$ are measured as a function of $t$. The $r^{04}_{1-1}$ and $\mathrm{Re}\,[r^{04}_{10}]$ matrix elements differ significantly from zero, thus confirming the violation of $s$-channel helicity conservation, with contributions from both single and double helicity-flip observed. The models considered are unable to describe the spin density matrix elements. The two-gluon model predicts far too large a probability of producing a longitudinally polarised $\rho$ meson, given by the $r^{04}_{00}$ matrix element. While the BFKL based model is able to describe the $r^{04}_{00}$ matrix element well, the prediction for $r^{04}_{1-1}$ is too negative and $\mathrm{Re}\,[r^{04}_{10}]$ has the wrong sign.

# Acknowledgements

We are grateful to the HERA machine group whose outstanding efforts have made this experiment possible. We thank the engineers and technicians for their work in constructing and maintaining the H1 detector, our funding agencies for financial support, the DESY technical staff for continual assistance and the DESY directorate for support and for the hospitality which they extend to the non DESY members of the collaboration. We are also grateful to R. Enberg, J. R. Forshaw, L. Motyka and G. Poludniowski for providing the results of the models and for useful discussions.

# References

[1] J. R. Forshaw and M. G. Ryskin, Z. Phys. C **68** (1995) 137 [hep-ph/9501376].

[2] J. Bartels, J. R. Forshaw, H. Lotter and M. Wüsthoff, Phys. Lett. B **375** (1996) 301 [hep-ph/9601201].

[3] S. Chekanov *et al.* [ZEUS Collaboration], Eur. Phys. J. C **26** (2003) 389 [hep-ex/0205081].

[4] A. Aktas *et al.* [H1 Collaboration], Phys. Lett. B **568** (2003) 205 [hep-ex/0306013].

[5] C. Adloff *et al.* [H1 Collaboration], Phys. Lett. B **541** (2002) 251 [hep-ex/0205107].

[6] C. Adloff *et al.* [H1 Collaboration], Phys. Lett. B **539** (2002) 25 [hep-ex/0203022].

[7] I. F. Ginzburg, S. L. Panfil and V. G. Serbo, Nucl. Phys. B **284** (1987) 685.

[8] D. Y. Ivanov, R. Kirschner, A. Schäfer and L. Szymanowski, Phys. Lett. B **478** (2000) 101 [Erratum-ibid. B **498** (2001) 295] [hep-ph/0001255].

[9] R. Enberg, J. R. Forshaw, L. Motyka and G. Poludniowski, JHEP **0309** (2003) 8 [hep-ph/0306232].

[10] G. G. Poludniowski, R. Enberg, J. R. Forshaw and L. Motyka, JHEP **0312** (2003) 2 [hep-ph/0311017].

[11] P. Ball and V. M. Braun, Nucl. Phys. B **543** (1999) 201 [hep-ph/9810475].

[12] J. R. Forshaw and G. Poludniowski, Eur. Phys. J. C **26** (2003) 411 [hep-ph/0107068].

[13] B. Cox, J. R. Forshaw and L. Lönnblad, JHEP **9910** (1999) 023 [hep-ph/9908464].

[14] R. Enberg, private communication.

[15] I. Abt *et al.* [H1 Collaboration], Nucl. Instr. Meth. A **386** (1997) 310 and 348.

[16] C. B. Gwilliam, PhD Thesis, The University of Manchester, 2006,
(available at http://www-h1.desy.de/publications/theses_list.html)

[17] F. Jacquet and A. Blondel, DESY 79-048 (1979) 377.

[18] P. Joos *et al.*, Nucl. Phys. B **113** (1976) 53.

[19] K. Schilling and G. Wolf, Nucl. Phys. B **61** (1973) 381.

[20] B. List and A. Mastroberardino, Proc. of the Workshop on Monte Carlo Generators for HERA Physics, eds. A. T. Doyle *et al.*, DESY-PROC-1999-02 (1999) 396.

[21] C. Adloff *et al.* [H1 Collaboration], Z. Phys. C **75** (1997) 607 [hep-ex/9705014].

[22] K. Goulianos, Phys. Rept. **101** (1983) 169.

[23] S. Eidelman *et al.* [Particle Data Group], Phys. Lett. B **592** (2004) 1.

[24] P. Söding, Phys. Lett. **19** (1966) 702.

[25] M. Ross and L. Stodolsky, Phys. Rev. **149** (1966) 1173.

[26] R. Brun *et al.*, CERN-DD/DD-84-1.

[27] J. Breitweg *et al.* [ZEUS Collaboration], Phys. Lett. B **487** (2000) 273 [hep-ex/0006013].

[28] T. J. Killian *et al.*, Phys. Rev. D **21** (1980) 3005.

[29] W. D. Shambroom *et al.*, Phys. Rev. D **26** (1982) 1.

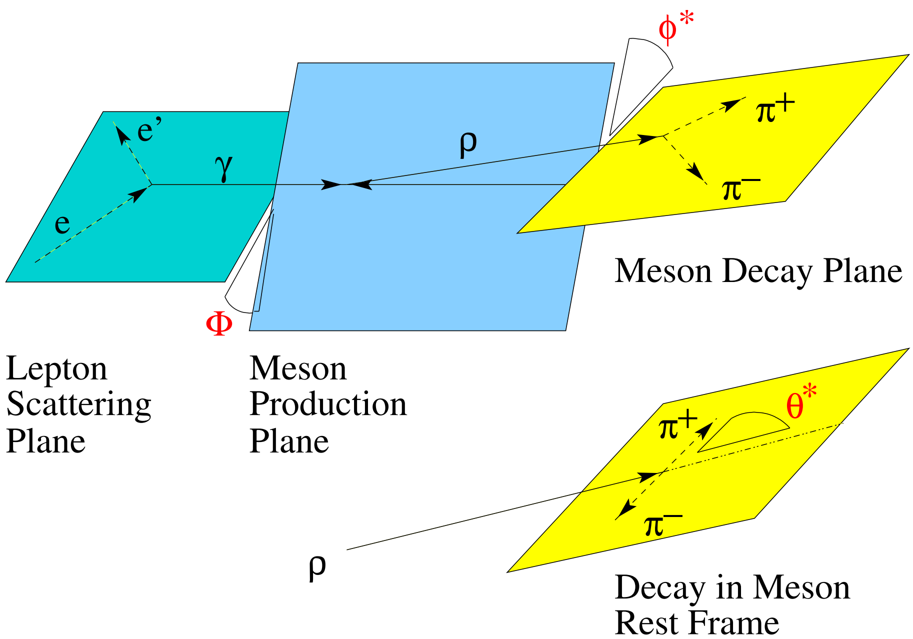


Figure 1: Production and decay angles used to analyse the polarisation of the $\rho$ meson.

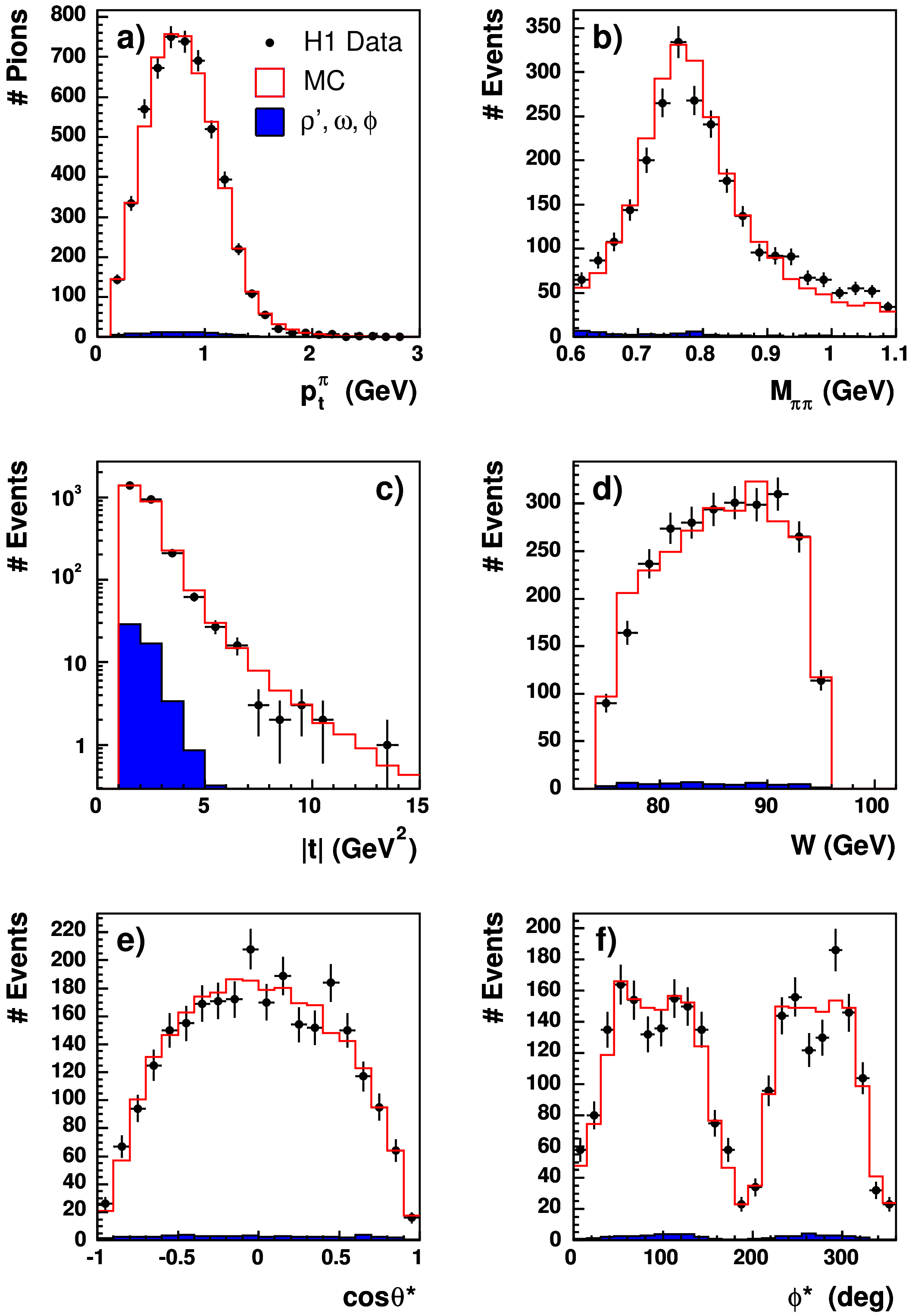


Figure 2: Distributions of the selected events in the kinematic domain (2) and the invariant mass range $0.6 < M_{\pi\pi} < 1.1$ GeV: a) transverse momentum of the pions; b) invariant mass of the two pions; c) modulus of the square of the four momentum transferred at the proton vertex $t$; d) photon-proton centre of mass energy $W$; e) cosine of the polar angle $\theta^*$ of the positively charged decay pion in the $\rho$ rest frame and f) its azimuthal angle $\phi^*$ the $\gamma p$ centre of mass frame. The points represent the data and the histograms show the Monte-Carlo predictions normalised to the data, including the $\omega$, $\phi$ and $\rho'$ backgrounds (filled histograms).

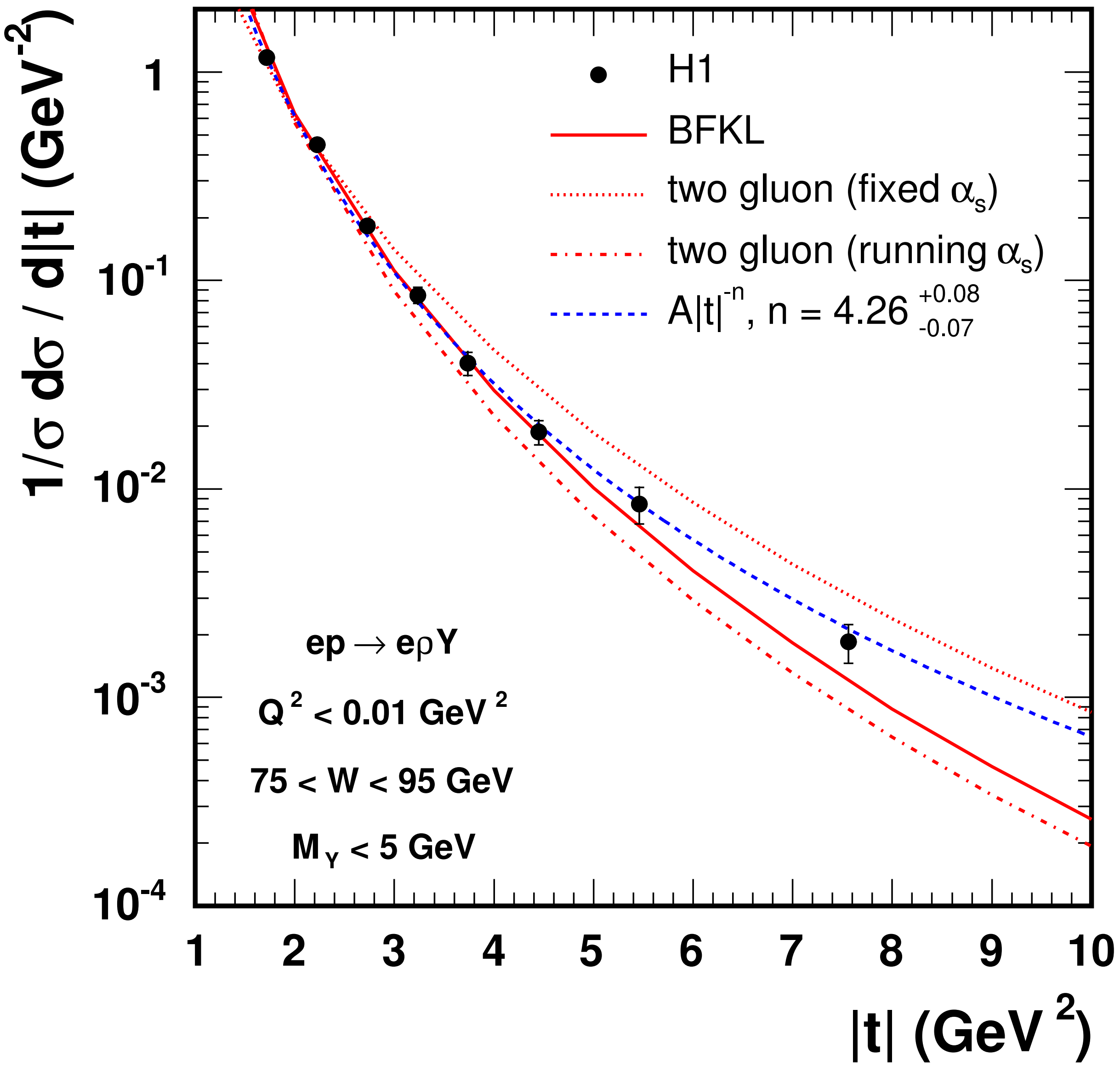


Figure 3: The $t$ dependence of the $ep \rightarrow e\rho Y$ cross section. The inner error bars show the dominating statistical errors, while the outer error bars represent the sum of the statistical and systematic errors added in quadrature. The dashed line is the result of a fit to a power law distribution $|t|^{-n}$, which results in a power $n = 4.26 \pm 0.06\,(\text{stat.})\,^{+0.06}_{-0.04}\,(\text{syst.})$. The full line shows the prediction from the BFKL model and the dotted and dashed-dotted lines show the predictions from the two-gluon model with fixed and running $\alpha_s$, respectively.

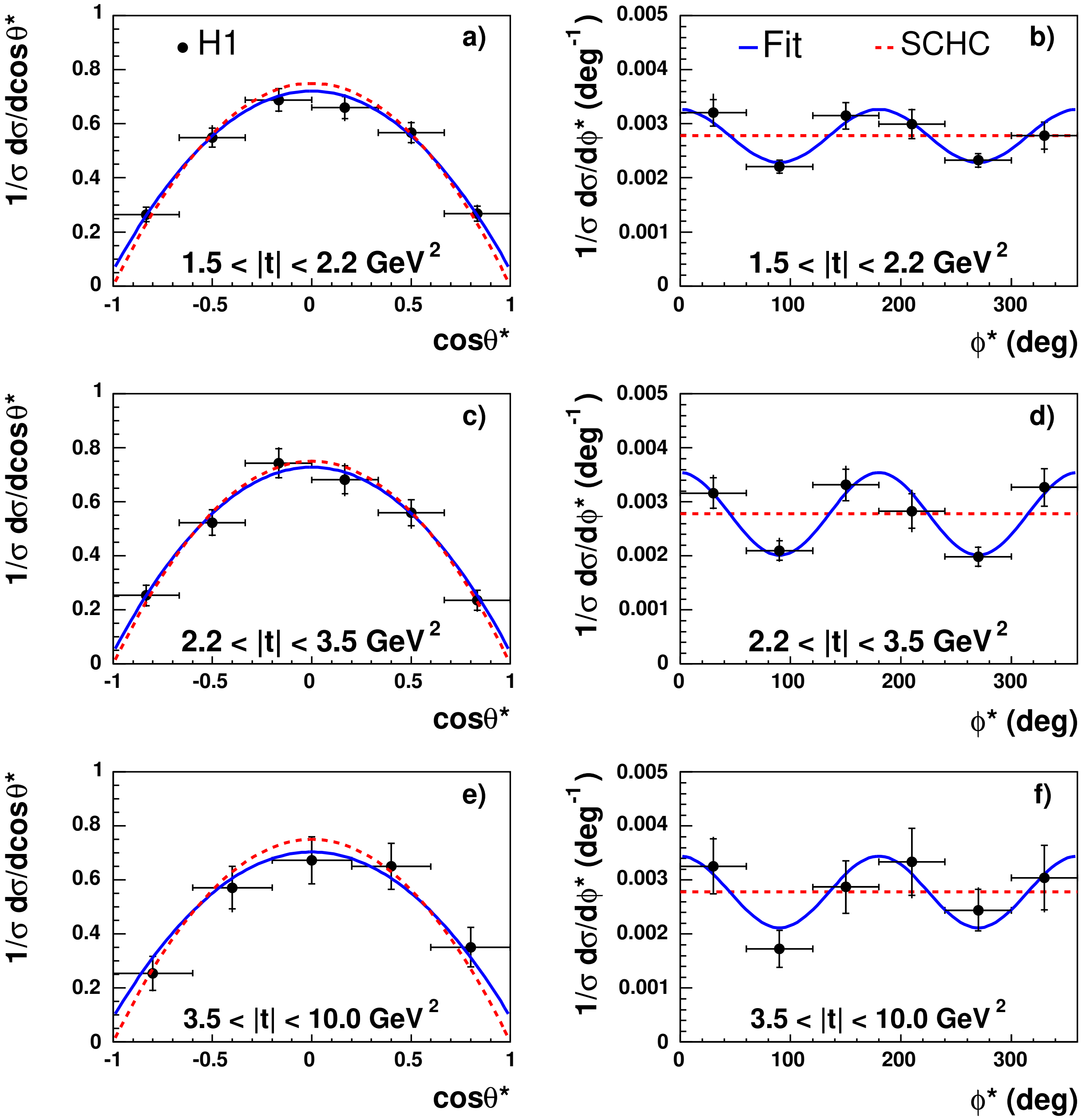


Figure 4: Normalised decay angular distributions for $\rho$ meson photoproduction in three bins of $|t|$. The left column (a,c,e) shows the polar distribution $\cos\theta^*$ and the right column (b,d,f) shows the azimuthal distribution $\phi^*$. The inner error bars show the statistical errors, while the outer error bars represent the sum of the statistical and systematic errors added in quadrature. The solid lines show the results of the two-dimensional fit to the data (see text). The dashed lines show the expectations for $s$-channel helicity conservation (SCHC).

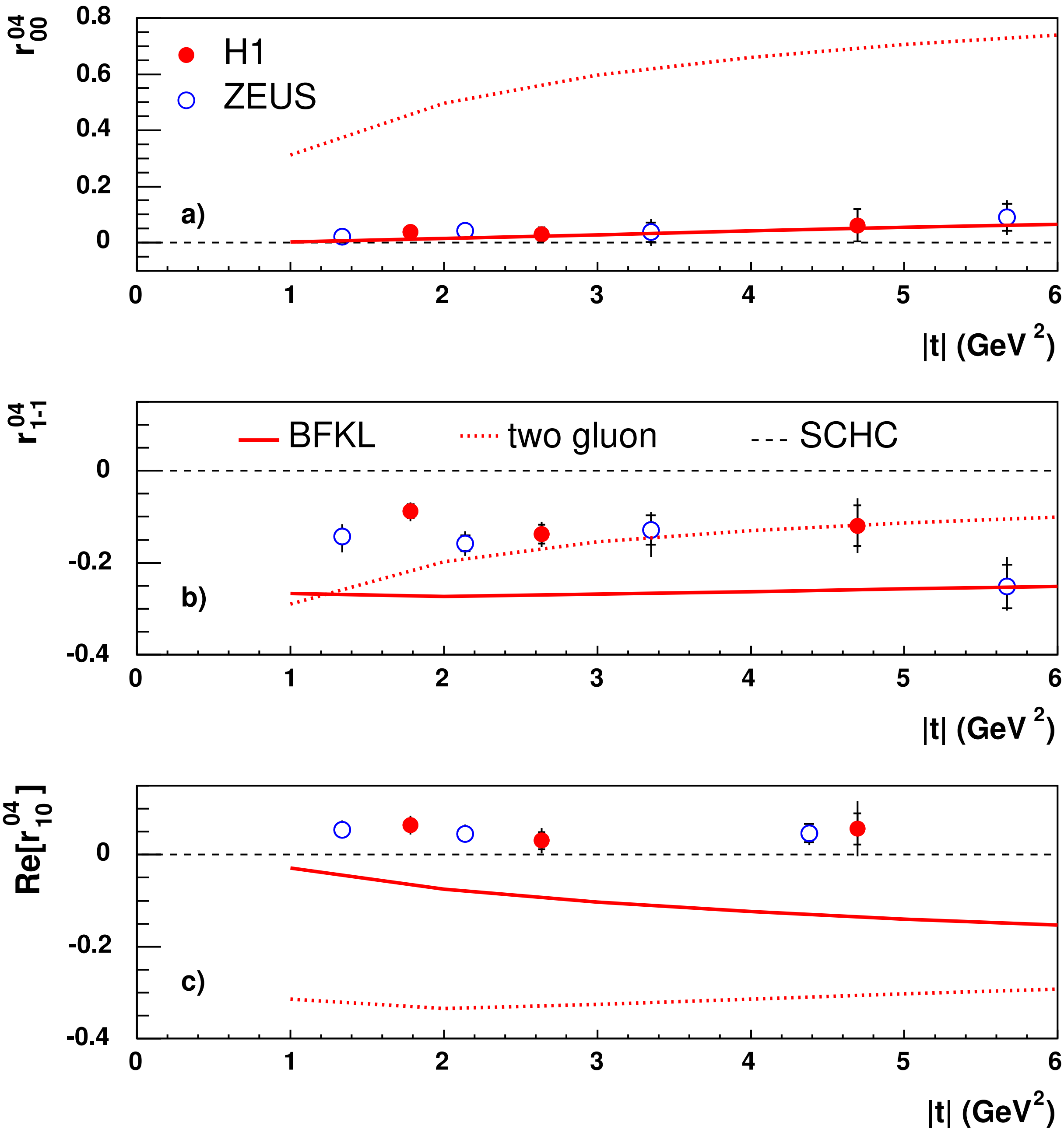


Figure 5: The three spin density matrix elements a) $r^{04}_{00}$, b) $r^{04}_{1-1}$ and c) $\mathrm{Re}\,[r^{04}_{10}]$ for $\rho$ meson photoproduction as a function of $|t|$ (full points) together with ZEUS measurements [3] (open points). The inner error bars show the statistical errors, while the outer error bars represent the sum of the statistical and systematic errors added in quadrature. The full lines show the predictions of the BFKL model and the dotted lines show the predictions of the two-gluon model. The dashed lines show the expectation from $s$–channel helicity conservation (SCHC).